Full Length Research Article

© 2025, Centre for Advanced Research in Agricultural Sciences
Research Journal of Agricultural Sciences
Volume 16; Issue 04 (Jul–Aug 2025); pp 374–383

ISSN: 0976-1675 (P)
ISSN: 2249-4538 (E)

Green Synthesis of Ag Doped CuO Nanoparticles using *Clerodendrum infortunatum* Leaf Extract and its Anticancer Activities against AGS Cancer Cells

H. R. Uma[1, 3] and Jessica Fernando*[2, 3]

[1] Research Scholar (Register No: 20113112032013) Department of Chemistry, V. O. Chidambaram College, Thoothukudi - 628 008, Tamil Nadu, India
[2] Associate Professor, Department of Chemistry, V. O. Chidambaram College, Thoothukudi - 628 008, Tamil Nadu, India
[3] Affiliated to Manonmaniam Sundaranar University, Abishekapatti - 627 012, Tamil Nadu, India

Received: 30 Jun 2025; Revised accepted: 05 Aug 2025

Abstract

This study reports the synthesis of copper oxide nanoparticles doped with silver (Ag) using a cost-effective, eco-friendly method that leverages *Clerodendrum infortunatum* leaf extract. A range of characterization techniques, including XRD, TEM, XPS, EDX, UV-Visible, and PL spectroscopy, were employed to analyze the nanoparticles. The XRD pattern confirmed the successful incorporation of Ag ions into the CuO monoclinic structure with high phase purity. TEM imaging revealed irregular and spherical shapes, while XPS measurements demonstrated effective silver incorporation into the CuO lattice. EDX spectroscopy verified the presence of Cu, Ag, and O, attesting to the purity of the prepared samples. The UV-Visible absorption spectra showed a larger optical band gap for Ag-doped CuO (1.43 eV) compared to bare CuO nanoparticles. Photoluminescence studies indicated an increase in PL emission intensity across the UV region upon silver ion addition. Furthermore, MTT assays revealed that Ag-doped CuO nanoparticles exhibited superior toxicity against the AGS human gastric adenocarcinoma cell line compared to pure CuO nanoparticles. These findings suggest that plant extract-mediated synthesis of pure CuO and Ag-doped CuO nanoparticles holds promise for biomedical applications.

***Key words*:** *Clerodendrum infortunatum* leaves, Anticancer activity, Cell viability, Optical band gap

The global human population is confronted with numerous pressing issues, including the pervasive threats of cancer, infectious diseases, and environmental pollution. Cancer, a complex and multifactorial disease, is marked by uncontrolled cell growth and the unchecked spread of abnormal cells, resulting in substantial mortality worldwide. With millions of new cases diagnosed annually, cancer remains a leading cause of death globally. Conventional cancer treatments, which often involve surgery, chemotherapy, and radiation, can be prohibitively expensive, time-consuming, and accompanied by debilitating side effects [1-2]. The escalating misuse and overuse of hazardous industrial chemicals have led to a surge in environmental pollution, posing a significant global challenge. The contamination of water bodies with toxic pollutants and chemical wastes has severe consequences for aquatic life and human health [3-4]. Moreover, the rise of antimicrobial resistance has become a pressing concern worldwide, rendering conventional treatments ineffective and resulting in prolonged illnesses and increased mortality rates. This growing threat necessitates urgent attention from researchers to develop novel, affordable, and highly effective antibiotics to combat antibiotic resistance [4]. The rapid advancement of nanoscience and nanotechnology has ushered in a new era of opportunities for manipulating particles at the nanoscale, with significant implications for technological and industrial applications. The unique properties of nanomaterials, stemming from their distinct size, diverse morphology, and high surface-to-volume ratio, make them particularly attractive [5]. Specifically, nanostructured metal oxides, such as ZnO [1], CuO [2], ZrO [6], SnO_2 [7], and TiO_2 [8], have emerged as potent antimicrobial agents, owing to their exceptional efficiency, high reactivity, low cost, ease of synthesis, notable optical band gap, and enhanced surface-to-volume ratio. Among nanostructured metal oxides, copper oxide (CuO) stands out due to its narrow optical band gap (1.7 eV) and p-type semiconducting properties, making it a versatile material for various applications, including superconductors [9], solar cells [10], photocatalysis [4], and biomedical fields [2]. To further enhance its physicochemical properties, doping CuO with suitable impurities has been explored, resulting in the creation of lattice defects and modulated charge carrier mobility [5]. Previous studies have investigated CuO doping with transition metals such as manganese (Mn), nickel (Ni), silver (Ag), zinc (Zn), iron (Fe), calcium (Ca), and cobalt (Co) [2], [4-5], [9-12]. Among the various transition metal dopants, silver (Ag) has garnered significant attention from researchers due to its potential in high-energy and biomedical applications [2]. Several physicochemical methods have been employed to

***Correspondence to:** Jessica Fernando, E-mail: jessivoc@yahoo.com

Citation: Uma HR, Fernando J. 2025. Green synthesis of Ag doped CuO nanoparticles using *Clerodendrum infortunatum* leaf extract and its anticancer activities against AGS cancer cells. *Res. Jr. Agril. Sci.* 16(4): 374-383.

fabricate metal-doped CuO nanoparticles, including co-precipitation [13], solid-state and microwave-assisted combustion methods [14], hydrothermal [15], sol-gel [16], and thermal decomposition [17]. However, these conventional techniques are often energy-intensive, costly, and environmentally hazardous, releasing toxic chemicals. Therefore, there is a growing need to develop an eco-friendly, stable, safe, cost-effective, and easily stored green synthesis approach that integrates green chemistry and natural products [18]. In recent years, the green fabrication of nanoparticles has emerged as an environmentally friendly solution for various applications, including biomedical, agricultural, and environmental remediation [19]. Plant extracts from various parts, such as peels, leaves, flowers, roots, seeds, and stems, have been utilized to synthesize nanoparticles, leveraging the secondary metabolites present in these plant materials [20]. These secondary metabolites in leaf extracts serve as reducing and stabilizing agents, facilitating the conversion of metal ions into metal oxide nanoparticles. Building on previous research, such as the phyto-mediated synthesis of zinc oxide nanoparticles from *Clerodendrum infortunatum* L. leaf extract and their antibacterial potential [21], this study explores the green synthesis of CuO and Ag-doped CuO nanoparticles using *Clerodendrum infortunatum* leaf extract. To the best of our knowledge, this is the first report on doping elements within CuO using this specific leaf extract. The synthesized nanoparticles were characterized using XRD, TEM, EDS, XPS, UV-Visible, and PL spectroscopy, and their anticancer activity was evaluated using MTT assays.

MATERIALS AND METHODS

The chemical reagents employed in this study were copper (II) nitrate and silver nitrate ($AgNO_3$), both of which were procured from SRL Chemicals with a guaranteed purity of 99%. All reagents used were of analytical grade and were utilized without additional purification. Furthermore, all aqueous solutions were prepared using double-distilled water to ensure optimal purity.

Preparation of leaf extract

Fresh leaves of *Clerodendrum infortunatum* were collected, thoroughly cleaned with tap water, and then rinsed repeatedly with double-distilled water. After drying, 30 g of the leaves were mixed with 150 mL of double-distilled water and heated to 80°C, resulting in a yellow-colored solution. The extract was then allowed to cool to room temperature, filtered using Whatman filter paper, and stored in the refrigerator for subsequent use.

Synthesis of pure copper oxide nanoparticles

A 5g quantity of copper nitrate was dissolved in 50 ml of double-distilled water. Subsequently, 10ml of the previously prepared leaf extract was added to the solution under constant stirring. To adjust the pH to 9, sodium hydroxide was added to the solution. The mixture was then subjected to magnetic stirring for 2 hours, resulting in the formation of a precipitate. The solution was left undisturbed for 24 hours to allow the precipitate to settle. The precipitate was then filtered, washed with a combination of double-distilled water and ethanol, and dried. Finally, the precipitate was muffled at 500°C for 2 hours to facilitate further characterization.

Synthesis of silver doped copper oxide nanoparticles

A solution was prepared by dissolving 5g of copper nitrate and 0.5g of silver nitrate ($AgNO_3$) in 50 ml of double-distilled water. Then, 10 ml of the previously prepared leaf extract was added to the solution under constant stirring. To adjust the pH to 9, sodium hydroxide was added to the solution. The mixture was then subjected to magnetic stirring for 2 hours, resulting in the formation of a precipitate. After allowing the solution to settle undisturbed for 24 hours, the precipitate was filtered, washed with a combination of double-distilled water and ethanol, and dried. Finally, the precipitate was calcined at 500°C for 2 hours to facilitate further characterization.

Characterization section

The crystal structure, phase determination, and average crystallite size of the synthesized samples were analyzed using X-ray diffraction (XRD) on a PANalytical X'Pert Pro instrument, equipped with Cu-Kα radiation (λ = 1.5406 Å) and operated at 40 kV and 30 mA. Transmission electron microscopy (TEM) was performed on a JEOL JEM-2100F instrument, operating at 200 kV, to obtain micrographs of the nanoparticles. X-ray photoelectron spectroscopy (XPS) analysis was conducted using a PHI 5000 Versa Probe 111 spectrometer, equipped with a high-performance Ar+ ion gun and optional C60 ion guns, to investigate the Zn 2p, O 1s, and Ag 3d peaks. The optical properties of the samples were evaluated using UV-Visible spectroscopy on a Perkin Elmer LAMBDA-35 spectrophotometer at room temperature. Photoluminescence (PL) spectra were collected using a Cary Eclipse Photoluminescence Spectrophotometer at room temperature.

Anticancer activity

The AGS (Human gastric adenocarcinoma) cell line was obtained from the National Centre for Cell Science (NCCS), Pune, India. The cells were cultured in DMEM/F12 medium supplemented with 10% fetal bovine serum (FBS) and 1% antibiotic-antimycotic solution in a humidified atmosphere with 5% CO2, 18-20% O_2 at 37°C. The cells were sub-cultured every 2 days, and the passage number used for this study was 37. For the assay, 200 µl of cell suspension was seeded in a 96-well plate at a density of 10,000 cells per well and allowed to grow for 24 hours. Test compounds were then added to the wells at various concentrations, and the plates were incubated for an additional 24 hours at 37°C in a 5% CO_2 atmosphere. Following incubation, the plates were removed, and the spent media was replaced with MTT reagent at a final concentration of 0.5 mg/ml. The plates were then incubated for 3 hours in the dark, after which the MTT reagent was removed, and 100 µl of solubilization solution (DMSO) was added. The plates were gently stirred, and the absorbance was measured at 570 nm using a spectrophotometer or ELISA reader. Cell viability was calculated using the following formula:

$$\text{Cell viability (\%)} = \frac{\text{OD sample mean}}{\text{OD control mean}} \times 100$$

RESULTS AND DISCUSSION

XRD analysis

X-ray diffraction (XRD) measurements were performed to identify the phases present in the prepared CuO and Ag-doped CuO nanoparticles. The XRD patterns, shown in Figure 1, reveal the polycrystalline nature of the samples with a single-phase structure. The diffraction patterns confirm the monoclinic structure of the CuO nanoparticles. Multiple diffraction peaks were observed at 32.84°, 35.20°, 38.69°, 48.82°, 53.43°, 58.18°, 62.27°, 66.20°, and 68.83°, which were attributed to the (-1 1

0), (0 0 2), (1 1 1), (-2 0 2), (0 2 0), (2 0 2), (-1 1 3), (-3 1 1), and (-2 2 0) planes, respectively [22]. A comparison with previous research revealed that the position and intensity of the planes' indices are in good agreement with the monoclinic structure, as assigned to JCPDS card No. 45-0937, indicating strong crystallinity [22]. Furthermore, the film exhibited a preferential orientation in the [111] direction [23]. In the case of Ag-doped CuO nanoparticles, the XRD pattern showed an increase in intensity of the peaks at 38.69° and a decrease in intensity of the peaks at 35.20°. Additionally, new diffraction peaks emerged at 44.75° and 64.65°, corresponding to the (200) and (220) planes, respectively, as assigned to JCPDS card No. 65-2871 [24], indicating good crystallinity related to Ag. The previous results confirm the successful doping of CuO thin film with Ag nanoparticles. The diffractograms reveal a preferential orientation along the (200) plane, suggesting that Cu^{2+} ions have been replaced by Ag ions without altering the crystalline structure or composition of CuO.

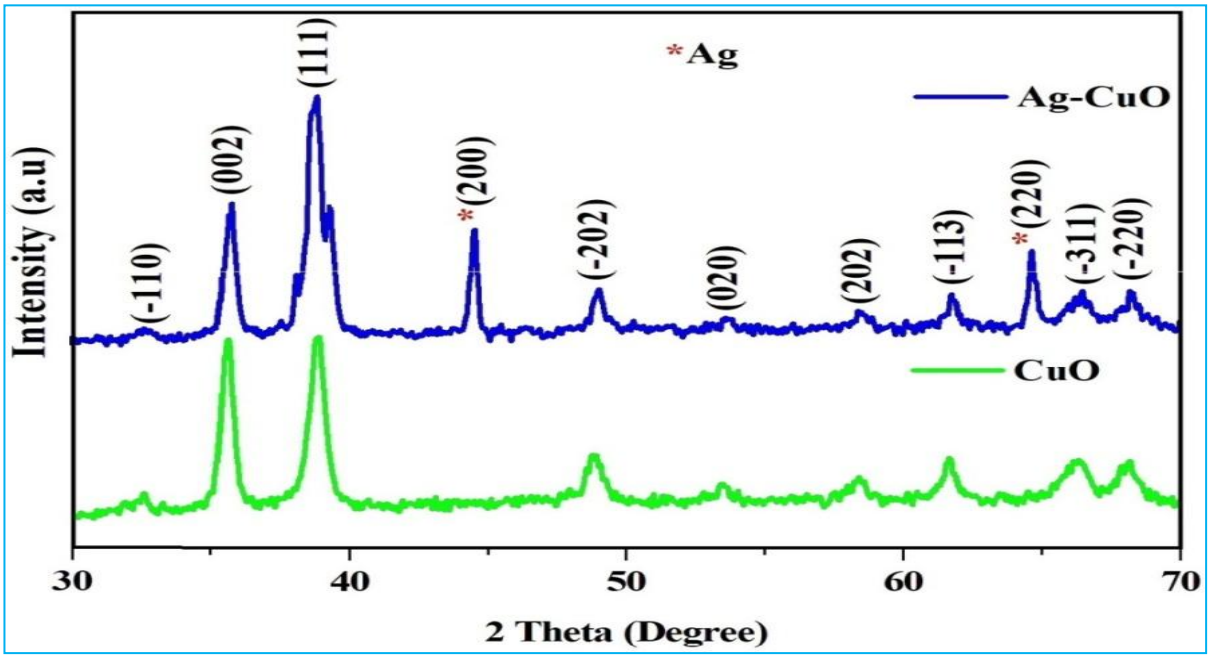

Fig 1 XRD spectra of pure CuO and Ag doped CuO nanoparticles

Furthermore, the XRD analysis did not detect any additional patterns beyond those corresponding to CuO or Ag in the synthesized nanoparticles. To deconvolute size and strain broadening, the Williamson-Hall (W-H) method was employed, which relates the peak width to the diffracting angle 2θ, yielding the following mathematical expression [25]:

$$\beta \cos\theta = \varepsilon\,(4\sin\theta) + \left(\frac{K\lambda}{D}\right) \qquad \ldots\ldots\ldots\ldots (1)$$

where λ (1.5406 Å) is the X-ray wavelength, ε is the average microstrain, θ is the Bragg diffraction angle, k is the shape factor (0.94), and β is the full width at half-maximum in radians. A plot of 4 sin θ vs. β cos θ was constructed for the synthesized nanoparticles. Fig. 2 displays the lattice strain for pure CuO and Ag-doped CuO nanoparticles, determined from the slope of the W-H plot. The W-H method revealed that the crystallite sizes of pure CuO and Ag-doped CuO nanoparticles are approximately 28.02 nm and 20.51 nm, respectively. Furthermore, the dislocation density (δ) was calculated using the Williamson and Smallman formula [26].

$$\delta = \frac{1}{D^2} \qquad \ldots\ldots\ldots\ldots (2)$$

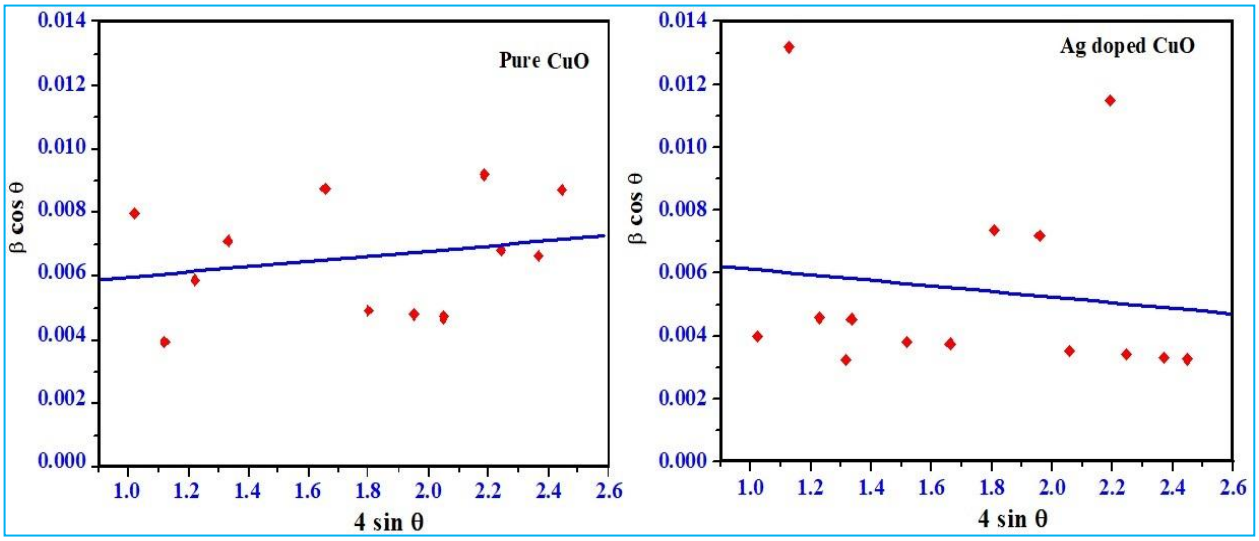

Fig 2 W-H plot for pure CuO and Ag doped CuO nanoparticles

The calculated values of particle size, strain, and dislocation density are summarized in (Table 1). A comparison of the dislocation density (δ) values reveals that Ag-doped CuO (2.37×10^{-3} nm^{-2}) exhibits a higher dislocation density than pure CuO (1.26×10^{-3} nm^{-2}). The decrease in crystallite size, as determined by the W-H method, is accompanied by an increase in dislocation density, suggesting that the stacking fault may decrease with increasing dislocation density [27]. Furthermore, the estimated strain (ε) values indicate that Ag-doped CuO (8.92×10^{-4}) experiences higher strain than pure CuO (8.26×10^{-4}).

Table 1 XRD parameters of pure CuO and Ag doped CuO nanoparticles

Sample	Williamsons Hall method		
	Average crystallite size D (nm)	Strain $\varepsilon \times 10^{-4}$	Dislocation density $\delta \times 10^{-3}$ nm^{-2}
Pure CuO	28.02	8.26	1.26
Ag doped CuO	20.51	8.92	2.37

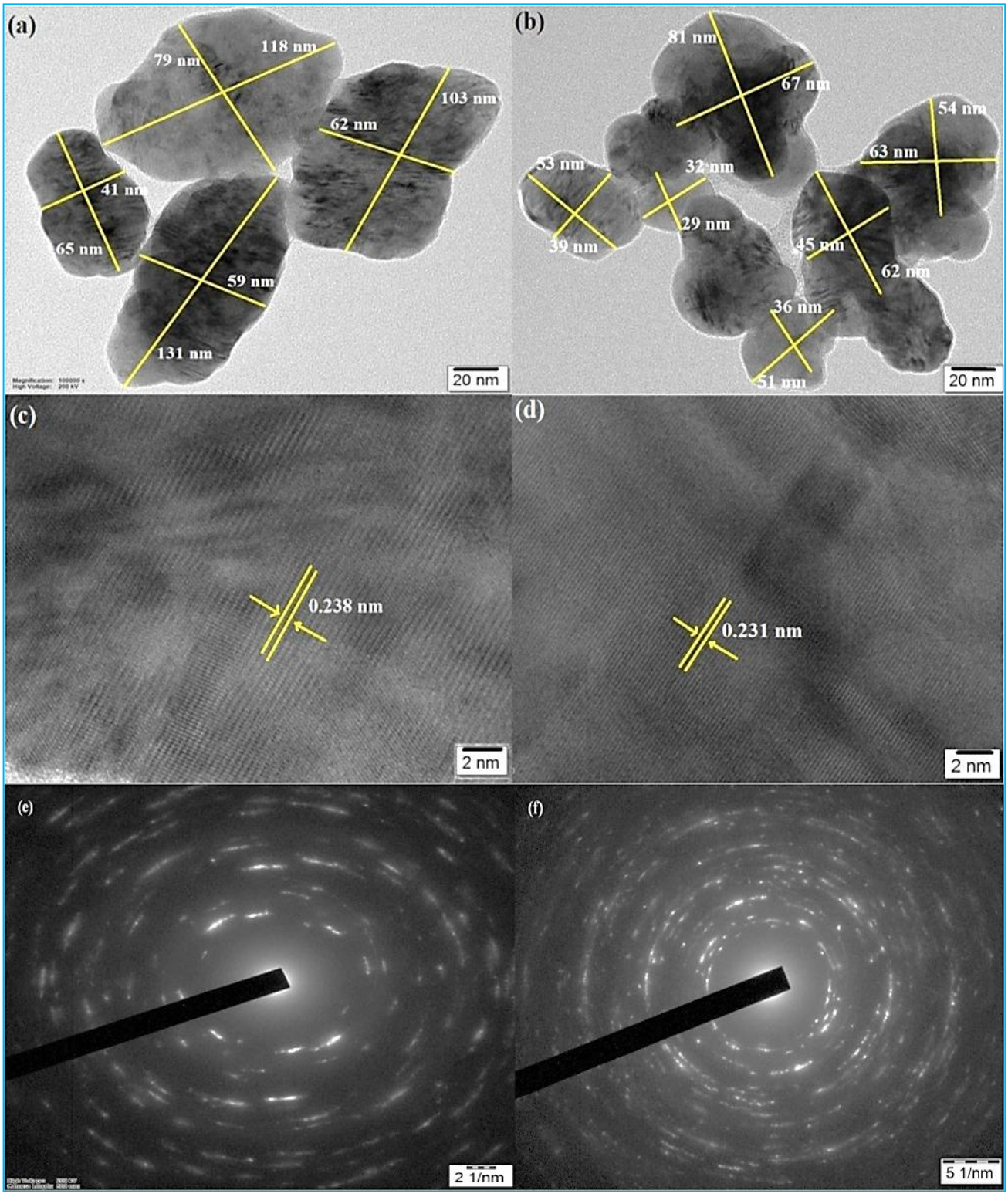

Fig 3(a-b) TEM image, (c-d) HRTEM image and SAED (e-f) of pure CuO and Ag doped CuO nanoparticles

TEM analysis

Transmission Electron Microscopy (TEM) analysis was performed on the synthesized nano powders, and the results are presented in (Fig 3a-b). The TEM images reveal that the CuO and Ag-doped CuO nanoparticles exhibit irregular and spherical shapes. The average length and width of the pure CuO nanoparticles were found to be 104.25 nm and 60.26 nm, respectively. In contrast, the average length and width of the Ag-doped CuO nanoparticles were determined to be 57.11 nm and 45.03 nm, respectively. High-resolution TEM (HRTEM) analysis showed lattice planar spacings of 0.238 nm for pure CuO and 0.231 nm for Ag-doped CuO nanoparticles, which is consistent with the literature value for the (111) plane of 0.23 nm [28]. The Selected Area Electron Diffraction (SAED) patterns of CuO and Ag-doped CuO nanoparticles, shown in (Fig 3c-f), exhibit diffraction rings with discrete diffraction spots, which is in good agreement with the observed XRD results and confirms the monoclinic structure of the CuO nanoparticles.

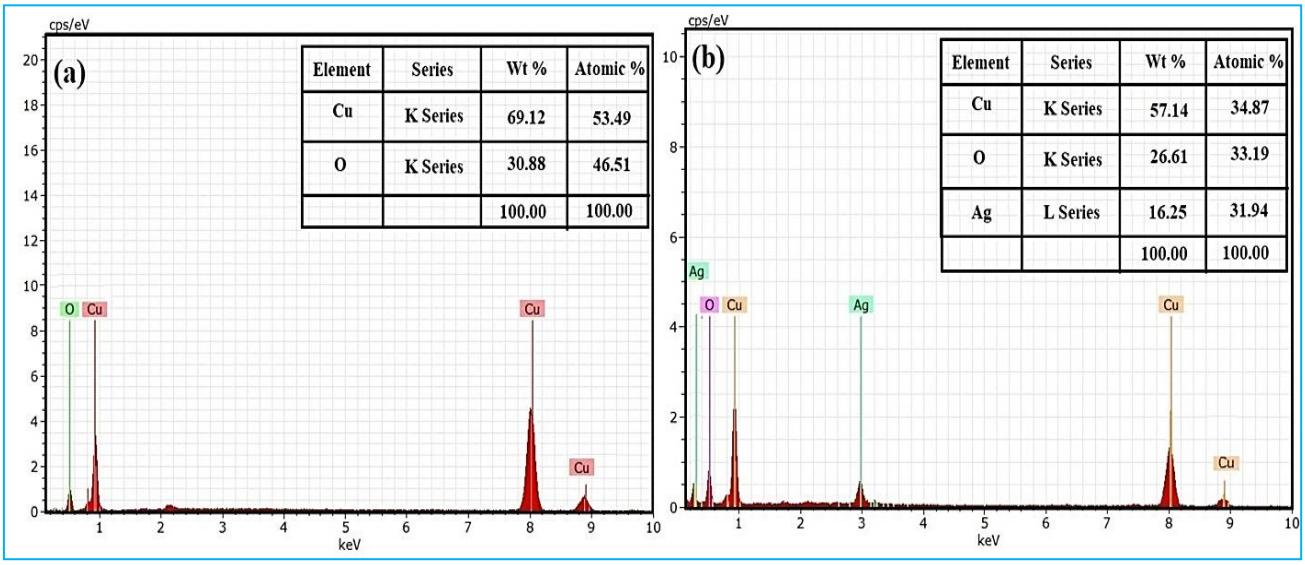

Fig 4 EDS spectra of (a) pure CuO and (b) Ag doped CuO nanoparticles

EDS spectral analysis

The (Fig 4) displays the Energy-Dispersive Spectroscopy (EDS) spectra of pure CuO and Ag-doped CuO nanoparticles. The EDS spectrum of CuO (Fig 4a) confirms the presence of copper (Cu) and oxygen (O) peaks, indicating the purity of the CuO nanoparticles. The inset of (Fig 4a) shows the chemical composition, with Cu and O present in weight percentages of 69.12% and 30.88%, respectively, and atomic percentages of 53.49% and 46.51%, respectively. In contrast, the EDS spectrum of Ag-doped CuO nanoparticles (Fig 4b) reveals the presence of a silver (Ag) peak, confirming the successful doping of Ag into the CuO matrix. The inset of (Fig 4b) shows the chemical composition, with Cu, O, and Ag present in weight percentages of 57.14%, 26.61%, and 16.25%, respectively, and atomic percentages of 34.87%, 33.19%, and 31.94%, respectively.

XPS spectra

To investigate the surface composition and chemical states of the prepared pure CuO and Ag-doped CuO nanoparticles, X-ray photoelectron spectroscopy (XPS) was employed. The high-resolution XPS spectra of pure CuO and Ag-doped CuO nanoparticles (Fig 5) reveal the presence of Cu 2p, O 1s, C 1s, and Ag 3d peaks. To correct for charging effects, all observed data were referenced to the C 1s peak, which typically appears at 283.28 eV. The presence of C 1s is attributed to adventitious carbon, which forms during atmospheric exposure [27]. Furthermore, the Cu 2p spectrum (Fig 6a) exhibits peaks corresponding to Cu 2p1/2 and Cu 2p3/2 at 953.92 eV and 933.88 eV, respectively. The separation between the Cu 2p3/2 peak and its satellite is approximately 9.71 eV, which is consistent with the values reported for copper materials, such as copper dihalides or CuO, with a d9 ground state electron configuration [29].

The XPS analysis confirms that the synthesized hybrid adsorbent contains copper oxide in the +2 oxidation state, consistent with previously reported values for CuO [29]. The O 1s XPS spectrum of the Ag-doped CuO nanoparticles (Fig 6b) reveals two peaks, indicating two oxygen states: lattice oxygen (Cu-O) at 529.76 eV and oxygen vacancies at 531.49 eV, corresponding to O^- and O^{2-} ions in the oxygen-deficient zone [27], [30]. The variation in peak intensity suggests changes in the number and concentration of oxygen vacancies [5]. The Ag 3d XPS spectrum (Fig 6c) exhibits two peaks, corresponding to metallic silver (Ag°) at 368.73 eV and silver ions (Ag^+) at 374.62 eV, consistent with previous reports [30]. These XPS results confirm the successful synthesis of Ag-doped CuO nanoparticles, corroborating the findings from EDX and XRD measurements.

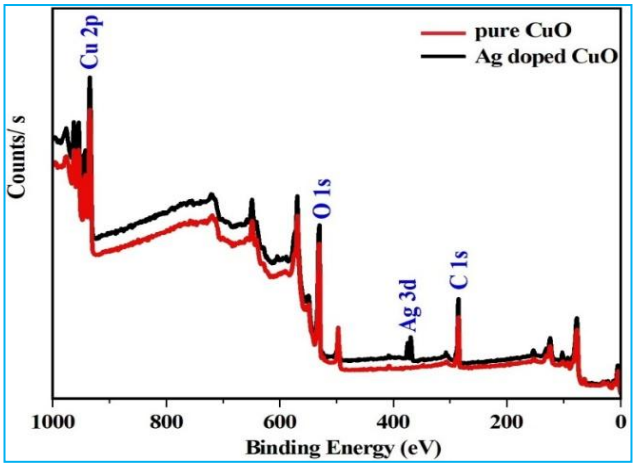

Fig 5 X-ray photoemission survey spectra of pure Cuo and Ag doped CuO nanoparticles

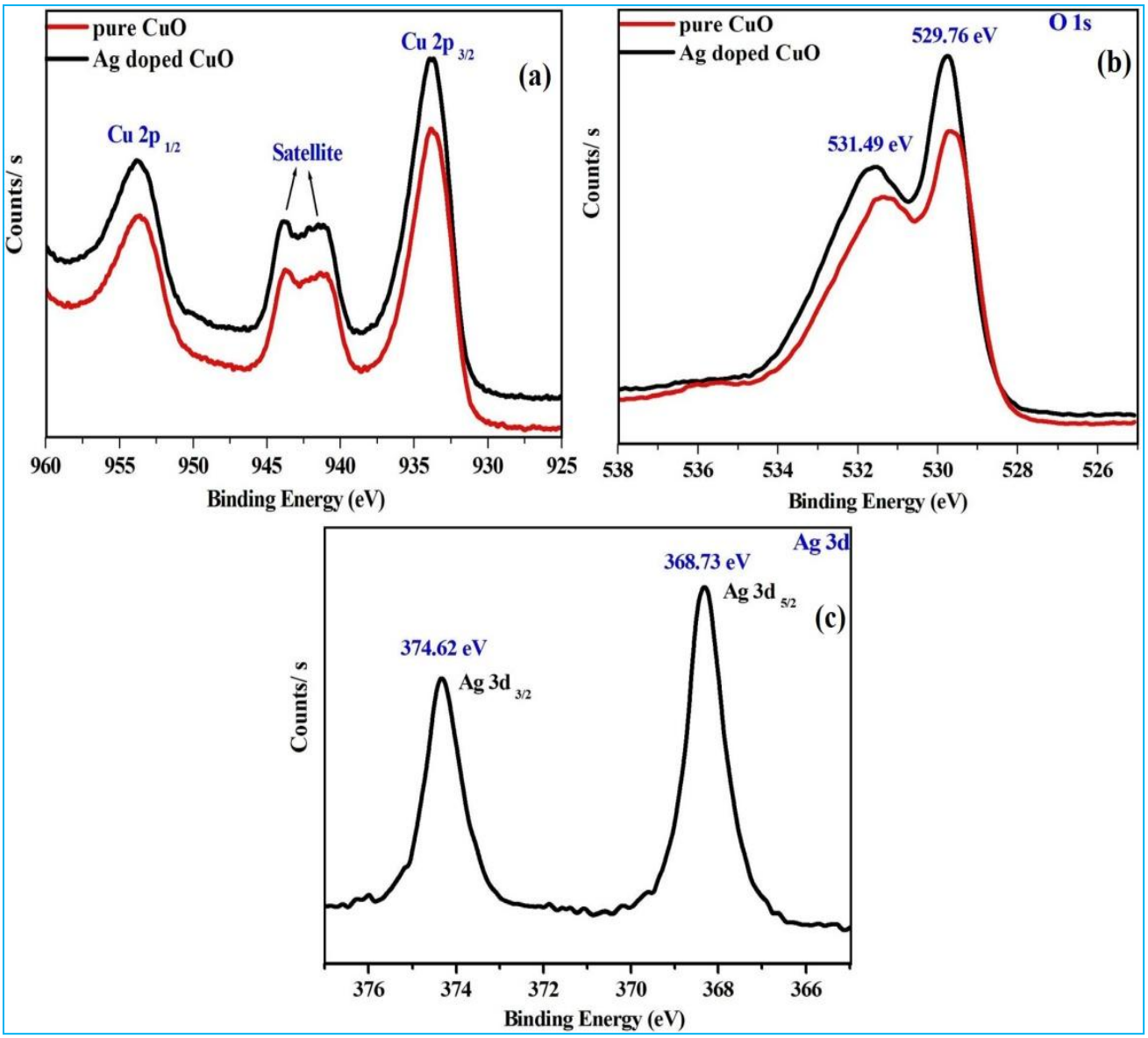

Fig 6 XPS spectrum of (a) Cu 2p (b) O 1s and (c) Ag 3d

UV-visible spectra

The absorption spectra of pure CuO and Ag-doped CuO nanoparticles are presented in (Fig 7). The optical properties of nanostructures are strongly influenced by the material's absorbance, which is related to the transition of charges from the valence band to the conduction band [31]. The absorption peaks for pure CuO and Ag-doped CuO nanoparticles are observed at 412 nm and 393 nm, respectively. Notably, the absorption peak of Ag-doped CuO nanoparticle is shifted to a lower wavelength compared to pure CuO nanoparticles, confirming the successful incorporation of Ag into the CuO lattice.

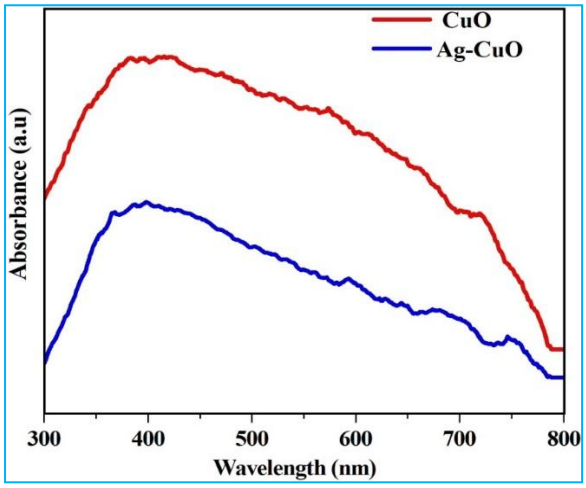

Fig 7 UV-visible absorbance spectra of pure CuO and Ag doped CuO nanoparticles

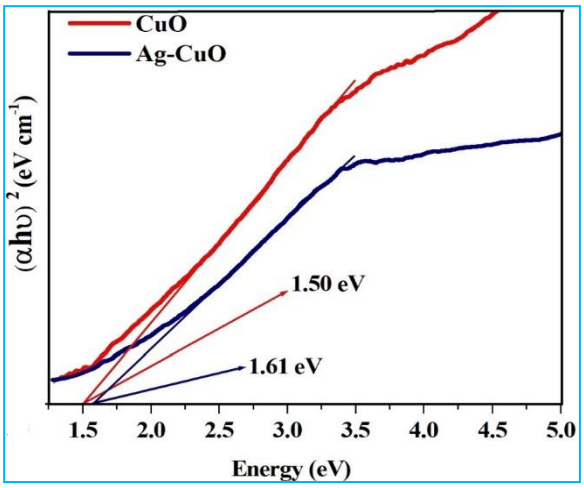

Fig 8 Tauc plot of pure CuO and Ag doped CuO nanoparticles

The Tauc equation [32] describes the relationship between the absorption coefficient (α) and photon energy (hν) for allowed direct transitions:

$$\alpha h\nu = C(h\nu - Eg)^n$$

where C is a constant, h is Planck's constant, υ is the frequency, Eg is the band gap energy, and n = 1/2 for direct band gap semiconductors.

The Tauc plot, shown in (Fig 8), illustrates the relationship between $(\alpha h\nu)^2$ and photon energy (hν). From this plot, the band gap energy (Eg) of pure CuO nanoparticles is determined to be 1.50 eV, which increases to 1.61 eV upon doping with Ag. This widening of the band gap energy can be attributed to the displacement of the Fermi level position into the conduction band, resulting from the increased carrier concentration [33].

PL spectra

The photoluminescence (PL) spectra of pure CuO and Ag-doped CuO nanoparticles were measured at room temperature, as shown in (Fig 9). The UV region (below 400 nm) corresponds to near-band-edge (NBE) emission, while the visible region (above 400 nm) is attributed to deep-level (DL) emissions, covering both regions within the UV-visible luminescence bands [34]. The addition of Ag dopant resulted in a decrease in emission intensity compared to pure CuO nanoparticles, likely due to defects such as single-ionized oxygen vacancies [35]. However, the increased electron-hole recombination in the valence band enhances the emission intensity of Ag-doped CuO nanoparticles. All the samples exhibit a broad UV emission band between 300-400 nm and three distinct emission peaks in the visible region. The strong UV emission band can be deconvoluted into two peaks at approximately 342 nm and 373 nm, which are attributed to near-band-edge (NBE) emission from free excitons in the conduction band [36]. Additionally, the violet emission peak at 406 nm is ascribed to the presence of interstitial copper. The radiative recombination between shallow donor (Cui) and deep acceptor (V_o) levels is believed to yield the observed violet emission around 439 nm [36]. Furthermore, the blue emission peak at 475 nm in both samples is attributed to defect-related emission or surface impurities, such as intrinsic defects, oxygen vacancies, surface states, and interstitial metal ions in the oxide, which are present in the CuO crystal and occurred during growth [37].

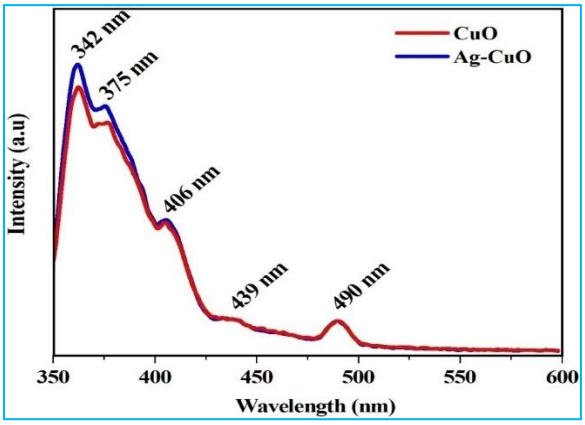

Fig 9 PL spectra of pure CuO and Ag doped CuO nanoparticles

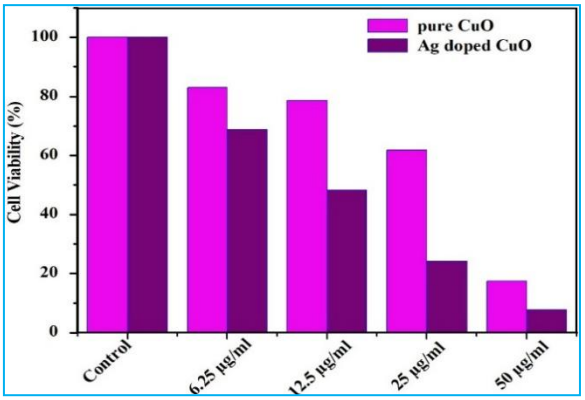

Fig 10 % cell viability values of AGS cells treated by different concentrations/ doses of pure CuO and Ag doped CuO nanoparticles after the incubation period of 24hrs by MTT assay

Anticancer activity

The anticancer activity of pure CuO and Ag-doped CuO nanoparticles against AGS (Human gastric adenocarcinoma) cells was evaluated using the MTT assay at various concentrations (6.25-500 µg/ml). The (Fig 10) shows the relative percent viability of AGS cells, indicating significant inhibition of cell viability by the nanoparticles. Notably, 100 µg/ml of the synthesized nanoparticles exhibited better inhibition of AGS cells compared to untreated cells. The results showed that increasing the concentration of pure CuO from 6.25µg/ml to 50µg/ml led to a progressive decrease in cell viability from 83.20% to 17.39%, respectively. In contrast, Ag-doped CuO nanoparticles demonstrated a more pronounced decrease in cell viability, from 68.80% to 7.73%, as the concentration increased from 6.25µg/ml to 50 µg/ml. These findings suggest that Ag-doped CuO nanoparticles exhibit higher anticancer activity than pure CuO nanoparticles. The cytotoxicity of CuO is attributed to factors such as particle size, ROS generation, and metal ion release [13], [38]. The concentration-dependent study revealed that Ag-doped CuO nanoparticles reduced AGS cell viability, likely due to their ability to penetrate cells and damage cancer cell function [39]. The Ag-doped CuO nanoparticles interact vigorously with the negatively charged surface of cancer cell membranes, leading to cell membrane breakage and destruction of cancerous cells. This process involves the intracellular release of silver and copper ions, which enhances cytotoxicity and enzyme disruption [40]. These findings suggest that Ag-doped CuO nanoparticles are a promising candidate for improved efficacy against cancerous cells. According to Akhtar *et al*. [41], the wide band gap behavior of metal-oxide nanoparticles plays a crucial role in ROS-mediated toxicity. The wide band gap Ag-doped CuO nanoparticles exhibit significant ROS-mediated cytotoxicity. Furthermore, our results indicate that Ag-doped nanoparticles mediated by *Clerodendrum infortunatum* leaf extract exhibit superior cytotoxic effects compared to pure nanoparticles, highlighting the impact of doped silver ions on enhancing induced cytotoxicity.

The MTT test results for human AGS cells treated with pure CuO and Ag-doped CuO nanoparticles are presented in (Fig 11). The figure illustrates that the samples inhibited AGS cell growth, with increasing concentrations/doses of 10µg/ml, 100 µg/ml, 300µg/ml, and 500µg/ml leading to decreased cell survival rates. The image reveals significant cell death after treatment with the prepared samples [42]. The MTT results indicate that Ag-doped CuO nanoparticles exhibited a higher likelihood of inducing cell death compared to pure CuO nanoparticles. Therefore, the synthesis of Ag-doped CuO nanoparticles mediated by *Clerodendrum infortunatum* leaf extract suggests that these nanoparticles could have potential chemotherapeutic effects, paving the way for their use in the development of anticancer drugs.

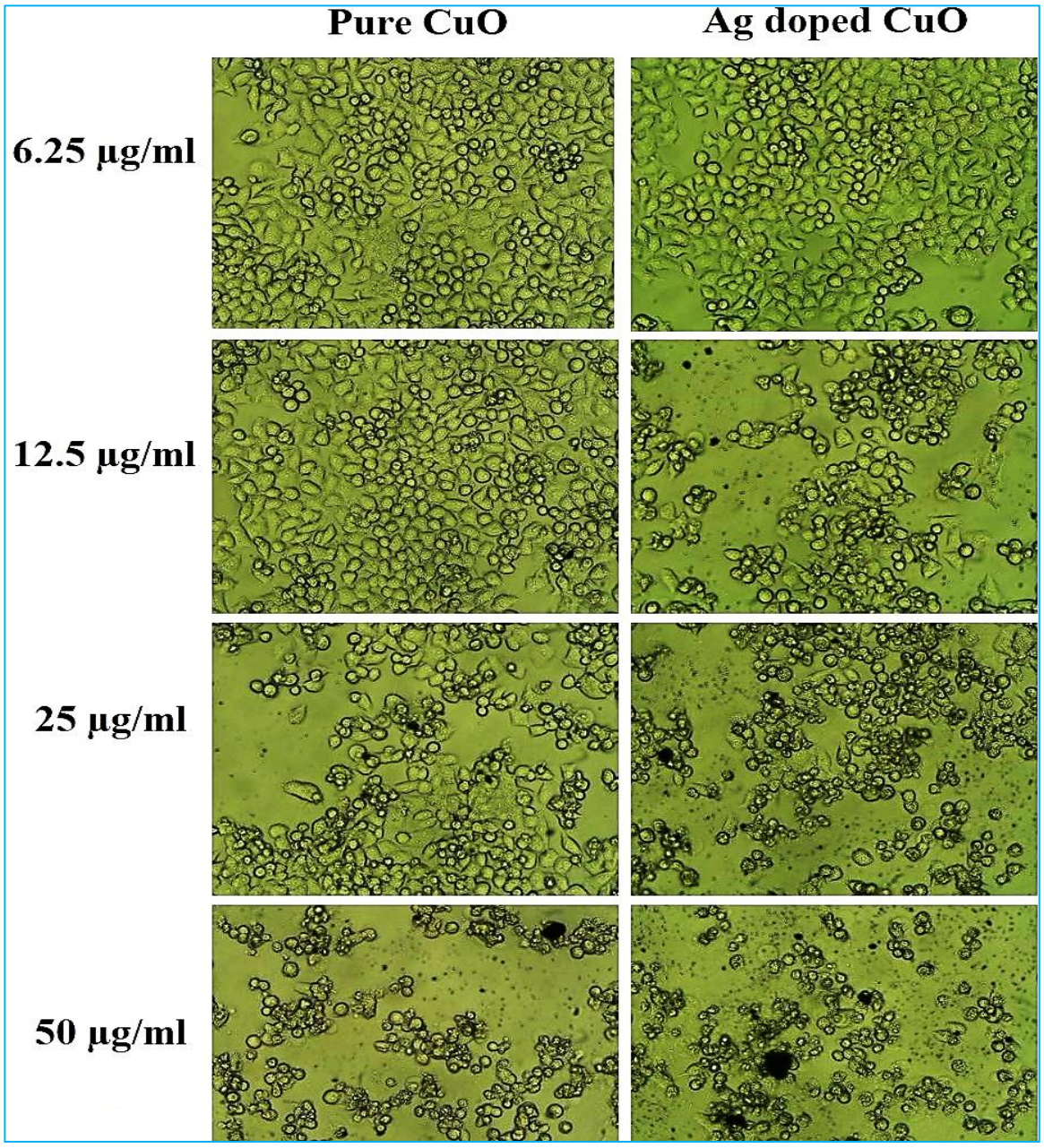

Fig 11 Cell numbers and viability evaluated using MTT staining after 24 h seeding (6.25µg/ml, 12.5µg/ml, 25 µg/ml and 50µg/ml)

CONCLUSION

In conclusion, this study successfully synthesized pure CuO and Ag-doped CuO nanoparticles using *Clerodendrum infortunatum* leaf extract as a reducing agent. The characterization of these nanoparticles using XRD, FTIR, SEM, EDX, and XPS revealed their crystalline structure, surface morphology, and elemental composition. The optical properties of the nanoparticles were studied using UV-Vis spectroscopy, which showed a blue shift in the absorption peak upon Ag doping. The photoluminescence study revealed a decrease in emission intensity upon Ag doping, indicating a reduction in defects. Furthermore, the MTT assay demonstrated the anticancer activity of the nanoparticles against AGS cells, with Ag-doped CuO nanoparticles exhibiting higher cytotoxicity than pure CuO nanoparticles. These findings suggest that Ag-doped CuO nanoparticles have potential applications in cancer therapy and open up new avenues for the development of novel anticancer agents.

Competing interests

The authors have no relevant financial or non-financial interests to disclose.

Funding

No funding was received to assist with the preparation of this manuscript.

Author contributions

H.R Uma conceived the research, designed experiments and wrote the paper. Jessica Fernando supervised, read and approved the manuscript.

Data availability statement

Data sets generated during the current study are available from the corresponding author on reasonable request.

Informed consent

Not Applicable.

Human and animal rights

Not Applicable.

LITERATURE CITED

1. Jakinala P, Lavudi HN, Angali N, Ganderla S, Inampudi KK, Andugulapati SB, Srinivas M, Katika MR. 2023. Green synthesis of ZnO-Ag nanocomposite using *Stenotaphrumsecundatum* grass extract: Antibacterial activity and anticancer effect in oral squamous cell carcinoma CAL 27 cells. *Inorganic Chemistry Communications* 152: 110735.
2. Preethi DRA, Prabhu S, Ravikumar V, Philominal A. 2022. Anticancer activity of pure and silver doped copper oxide nanoparticles against A549 Cell line. *Materials Today Communication* 33: 104462.
3. Sinha A, Sahu SK, Biswas S, Mandal M, Mandal V, Ghorai TK. 2022. Green approach to synthesize MnxZn1−xO nanocomposite with enhanced photocatalytic, fluorescence and antibacterial activity. *Current Research in Green Sustainable Chemistry* 5: 100244.
4. Vindhya PS, Kavitha VT. 2022. Leaf extract mediated synthesis of Mn doped CuO nanoparticles for antimicrobial, antioxidant and photocatalytic applications. *Chemical Papers* 77: 2407.
5. Vindhya PS, Kavitha VT. 2023. A comprehensive study on photocatalytic, antimicrobial, antioxidant and cytotoxicity effects of biosynthesized pure and Ni doped CuO nanoparticles. *Inorganic Chemistry Communications* 150: 110472.
6. Balaji S, Mandal BK, Ranjan S, Dasgupta N, Chidambaram R. 2017. Nano-zirconia – Evaluation of its antioxidant and anticancer activity. *Journal of Photochemistry and Photobiology* B 170: 125.
7. Alanazi S, Alaizeri ZM, Lateef R, Madkhali N, Alharbi A, Ahamed M. 2023. Zn doping improves the anticancer efficacy of SnO_2 nanoparticles. *Applied Science* 13: 12456.
8. Mbenga Y, Adeyemi JO, Mthiyane DMN, Singh M, Onwudiwe DC. 2023. Green synthesis, antioxidant and anticancer activities of TiO2 nanoparticles using aqueous extract of Tulbhagia violacea. *Results Chemistry* 6: 101007.
9. Iram F, Mustafa GM, Ali G, Ahmad H, Ramay SM, Iqbal Z, Atiq S. 2023. Transition metal (Zn, Mn, and Ni) incorporated CuO nanostructures for supercapacitor applications. *Jr. Energy Storage* 73: 108829.
10. Iqbal M, Ali A, Ahmad KS, Rana FM, Khan J, Khan K, Hussain K. 2019. Synthesis and characterization of transition metals doped CuO nanostructure and their application in hybrid bulk heterojunction solar cells. *SN Applied Science* 1: 647.
11. Saumya, Dasauni K, Nailwal TK, Voddumalla S, Nenavathu BP. 2023. Facile synthesis of Ca doped CuO nanoparticles and their investigation in antibacterial efficacy. *Biologia* 78: 903.
12. Sathyananda HM, Prashanth PA, Prashanth GK, Dileep MS, Prabhu SRB, Nagabhushana BM, Shivakumara C, Nagendra HG. 2022. Evaluation of antimycobacterial, antioxidant, and anticancer activities of CuO nanoparticles through cobalt doping. *Applied Nanoscience* 12: 79.
13. Jan T, Iqbal J, Farooq U, Gul A, Abbasi R, Ahmad I, Malik M. 2015. Structural, Raman and optical characteristics of Sn doped CuO nanostructures: A novel anticancer agent. *Ceramics International* 41: 13074.
14. Rejith SG, Krishnan C. 2023. Optical characterizations of Zn-doped CuO nanoparticles. *Sciencia Acta Xaveriana* 4: 91.
15. Mohebbi S, Molaei S, Azar ARJ. 2013. Preparation and study of Sn-doped CuO nanoparticles as semiconductor. *Journal of Applied Chemistry* 8: 27.
16. Amri SA, Ansari MS, Rafique S, Aldhahri M, Rahimuddin S, Azam A, Memic A. 2015. Ni doped CuO nanoparticles: Structural and optical characterizations. *Current Nanoscience* 11: 1.
17. Shaghaghi Z, Amani-Ghadim AR, Seraji M. 2020. Structural properties and photocatalytic degradation efficiency of CuO and erbium doped CuO nanostructures prepared by thermal decomposition of some Cu-salophen type complexes as precursors. *Materials Chemistry and Physics* 243: 122635.
18. Vindhya PS, Jeyasingh T, Kavitha VT. 2019. Dielectric properties of copper oxide nanoparticles using *Annona muricata* leaf. *AIP Conference Proceedings* 2162: 020021.
19. Ameen F. 2022. Optimization of the synthesis of fungus-mediated bi-metallic Ag-Cu nanoparticles. *Applied Science* 12: 1384.
20. Singh R, Dutta S. 2017. Synthesis and characterization of solar photoactive TiO2 nanoparticles with enhanced structural and optical properties. *Adv. Powder Technology* 29: 211.
21. Kumar S, Bithel N, Kumar S, Kishan, Sen M, Banerjee C. 2024. Phyto-mediated synthesis of zinc oxide nanoparticles from *Clerodendrum infortunatum* L. leaf extract and evaluation of antibacterial potential. *South Africa Jr. of Botany* 164: 146.
22. Menazea AA, Mostafa AM. 2020. Ag doped CuO thin film prepared via pulsed laser deposition for 4-nitrophenol degradation. *Jr. Environ. Chem. Engineering* 8: 104104.
23. Das S, Alford TL. 2013. Structural and optical properties of Ag-doped copper oxide thin films on polyethylene naphthalate substrate prepared by low temperature microwave annealing. *Jr. Appl. Physics* 113: 244905.
24. Menazea AA. 2020. Femtosecond laser ablation-assisted synthesis of silver nanoparticles in organic and inorganic liquids medium and their antibacterial efficiency. *Radiat. Phys. Chemistry* 168: 108616.
25. Samuel J, Suresh S, Shabna S, Vinita VS, Ananth NJ, Shinu PMS, Mariappan A, Simon T, Samson Y, Biju CS. 2022. Characterization and antibacterial activity of Ti doped ZnO nanorods prepared by hydrazine assisted wet chemical route. *Physica E: Low Dimensional Systems Nanostructures* 143: 115374.
26. Clement Singh CJ, Samuel J, Biju CS, Dhas SSJ, Jude Dhas SS, Usharani S. 2023. Effect of Sn doping on the structural, photoluminescence, ultraviolet filtering and antibacterial activity of ZnO nanorods. *Optical and Quantum Electronics* 55: 1072-1093.
27. Ravi A, Samuel J, Dhas SSJ, Usharani S, Simon T, Kumar DS, Vijitha SKJ, Sivakumar A, Kumar RS, Biju CS. 2024. Structural, morphological, optical and antibacterial performances of rare earth (Sm)-doped ZnO nanorods. *Journal of Rare Earths* 42(4).
28. Gupta K, Bersani M, Darr JA. 2016. Highly efficient electro-reduction of CO_2 to formic acid by nano-copper. *Journal of Materials Chemistry* A 4: 13786.
29. Boruban C, Esenturk EN. 2018. Activated carbon-supported CuO nanoparticles: a hybrid material for carbon dioxide adsorption. *Journal of Nanoparticle Research* 20: 59.
30. Iqbal S, Javed M, Bahadur A, Qamar MA, Ahmad M, Shoaib M, Raheel M, Ahmad N, Akbar MB, Li H. 2020. Controlled synthesis of Ag doped CuO nanoparticles as a core with poly (acrylic acid) microgel shell for efficient removal of methylene blue under visible light. *Jr. Mater. Sci. Materials in Electronics* 31: 8423.

31. Fangab J, Xuan Y. 2017. Investigation of optical absorption and photothermal conversion characteristics of binary CuO/ZnO nanofluids. *RSC Adv*. 7: 56023.
32. Mohammadikish M, Akradi AA. 2019. Synthesis and optical band gap determination of CuO nanoparticles from salen-based infinite coordination polymer nanospheres. *Mater. Res. Express* 6: 045013.
33. Samuel J, Shaji JE, Dhas SSJ, Suresh S, Vinita VS, Biju CS. 2023. UV-blocking performance and antibacterial activity of Cd, Ba co-doped ZnO nanomaterials prepared by a facile wet chemical method. *Surface and Interface Analysis* 1: 1.
34. Samuel J, Rajesh TSF, Biju CS, Dhas SSJ, Usharani S. 2023. Synthesis, structural, photoluminescence, ultraviolet blocking and antibacterial performances of Ba-doped ZnO nanostructures. *Results Opt*. 12: 100482-100489.
35. Pramothkumar A, Senthilkumar N, Gnana Malar KCM, Meena M, Potheher IV. 2019. A comparative analysis on the dye degradation efficiency of pure, Co, Ni and Mn doped CuO nanoparticles. *Journal of Material Science: Materials in Electronics* 30: 19043.
36. Gopalakrishnan R, Ashokkumar M. 2021. Rare earth metals (Ce and Nd) induced modifications on structural, morphological, and photoluminescence properties of CuO nanoparticles and antibacterial application. *Journal of Molecular Structure* 1244: 131207.
37. Siddiqui H, Parra MR, Malik MM, Haque FZ. 2018. Structural and optical properties of Li substituted CuO nanoparticles. *Optical and Quantum Electronics* 50: 260.
38. Wongrakpanich A, Mudunkotuwa IA, Geary SM, Morris AS, Spitz DR, Mapuskar KA, Grassian VH, Salem AK. 2016. Size-dependent cytotoxicity of copper oxide nanoparticles in lung epithelial cells. *Environmental Science: Nano* 3: 365.
39. Ullah A, Saadullah M, Alvi F, Sherin L, Ali A, Shad NA, Javed Y, Sajid MM, Yasin G, Abbas W. 2022. Synergistic effect of silver doped ZnO nanomaterials enhances the anticancer potential against A459 lung cancer cells. *Journal of King Saud University – Science* 34: 101724.
40. Pandiyan N, Murugesan B, Sonamuthu J, Samayanan S, Mahalingam S. 2019. [BMIM] PF_6 ionic liquid mediated green synthesis of ceramic SrO/CeO_2 nanostructure using *Pedalium murex* leaf extract and their antioxidant and antibacterial activities. C*eramics International* 45: 12138.
41. Akhtar MJ, Alhadlaq HA, Alshamsan A, Khan MAM, Ahamed M. 2015. Aluminum doping tunes band gap energy level as well as oxidative stress-mediated cytotoxicity of ZnO nanoparticles in MCF-7 cells. *Scientific Reports* 5: 13876.
42. Ahamed M, Akhtar MJ, Khan MAM, Alhadlaq HA. 2022. Enhanced anticancer performance of eco-friendly-prepared MoZnO/RGO nanocomposites: Role of oxidative stress and apoptosis. *ACS Omega* 7: 7103.